



<http://www.diva-portal.org>

This is the published version of a paper published in *Journal of Chemical Physics*.

Citation for the original published paper (version of record):

Rander, T., Lindblad, A., Bradeanu, I., Öhrwall, G., Svensson, S. et al. (2014)  
Suppression of the molecular ultra-fast dissociation in bromomethane clusters.  
*Journal of Chemical Physics*, 141: 224305  
<http://dx.doi.org/10.1063/1.4903455>

Access to the published version may require subscription.

N.B. When citing this work, cite the original published paper.

Permanent link to this version:

<http://urn.kb.se/resolve?urn=urn:nbn:se:uu:diva-241035>

Copyright (2015) AIP Publishing. This article may be downloaded for personal use only. Any other use requires prior permission of the author and AIP Publishing.

The following article appeared in *Journal of Chemical Physics* 2015:141, 224305 and may be found at <http://dx.doi.org/10.1063/1.4903455>.

**Suppression of the molecular ultra-fast dissociation in bromomethane clusters**

T. Rander, A. Lindblad, I. Bradeanu, G. Öhrwall, S. Svensson, and O. Björneholm

Citation: *The Journal of Chemical Physics* **141**, 224305 (2014); doi: 10.1063/1.4903455

View online: <http://dx.doi.org/10.1063/1.4903455>

View Table of Contents: <http://scitation.aip.org/content/aip/journal/jcp/141/22?ver=pdfcov>

Published by the [AIP Publishing](#)

---

**Articles you may be interested in**

[Simulations of the dissociation of small helium clusters with ab initio molecular dynamics in electronically excited states](#)

*J. Chem. Phys.* **140**, 134306 (2014); 10.1063/1.4869193

[The dissociative chemisorption of methane on Ni\(111\): The effects of molecular vibration and lattice motion](#)

*J. Chem. Phys.* **138**, 174705 (2013); 10.1063/1.4802008

[Communication: Quasiclassical trajectory calculations of correlated product-state distributions for the dissociation of \(H<sub>2</sub>O\)<sub>2</sub> and \(D<sub>2</sub>O\)<sub>2</sub>](#)

*J. Chem. Phys.* **135**, 151102 (2011); 10.1063/1.3655564

[A computational study of ultrafast acid dissociation and acid-base neutralization reactions. I. The model](#)

*J. Chem. Phys.* **133**, 044108 (2010); 10.1063/1.3461162

[Addition of water, methanol, and ammonia to Al<sub>3</sub>O<sub>3</sub> – clusters: Reaction products, transition states, and electron detachment energies](#)

*J. Chem. Phys.* **122**, 214309 (2005); 10.1063/1.1926279

---

 **AIP** | APL Photonics

*APL Photonics* is pleased to announce  
**Benjamin Eggleton** as its Editor-in-Chief



# Suppression of the molecular ultra-fast dissociation in bromomethane clusters

T. Rander,<sup>1</sup> A. Lindblad,<sup>1</sup> I. Bradeanu,<sup>1</sup> G. Öhrwall,<sup>2</sup> S. Svensson,<sup>1</sup> and O. Björneholm<sup>1</sup>

<sup>1</sup>Department of Physics, Uppsala University, P.O. Box 530, SE-751 21 Uppsala, Sweden

<sup>2</sup>MAX lab, Lund University, P.O. Box 118, SE-221 00 Lund, Sweden

(Received 16 October 2014; accepted 24 November 2014; published online 9 December 2014)

We address the influence of clustering on the ultra-fast dissociation of bromomethane. Valence and core photo-electron spectroscopy, partial electron yield absorption, and resonant Auger spectroscopy have been used together with *ab initio* calculations to investigate the properties of the ultra-fast dissociation. The ratio of ultra-fast dissociation of molecules in clusters as compared to free molecules is determined to be significantly reduced. We propose partial delocalization of the excited electronic state as being responsible for this behavior. © 2014 AIP Publishing LLC. [<http://dx.doi.org/10.1063/1.4903455>]

## I. INTRODUCTION

Ultra-fast dissociation (UFD) upon core excitation is a well known process in many molecular systems.<sup>1–6</sup> In such a process, a core electron is excited into an anti-bonding orbital. For some molecules, the core-excited state is anti-bonding to such a degree that the dissociation of the molecule will take place on the same time-scale as the electronic Auger decay. As a consequence, a fraction of the Auger decays occur in fragments of molecules, or as in the case of bromomethane in free Br atoms. It has been shown that the UFD process remains fairly unchanged in oxygen clusters in comparison to free molecules.<sup>7</sup> Since oxygen clusters are bonded mainly by van der Waals and quadrupole forces, the interaction between the constituent molecules is comparatively weak. In the present work, we aim to study the influence of stronger inter-molecular interactions on the UFD process. To this end, we have performed measurements on bromomethane clusters, which are bonded by dipole-dipole interaction as well as van der Waals forces.

The  $3d \rightarrow 4a_1$  core excitation in molecular bromomethane has been the subject of several studies.<sup>2,8–10</sup> These investigations have been performed using near-edge X-ray absorption fine structure (NEXAFS) spectroscopy and resonant Auger spectroscopy (RAS), and have focused on describing the character of the core excited state. Some recent studies of chloromethane, which is valence isoelectronic with bromomethane, and of larger molecules such as 1-bromo-2-chloroethane, utilizing a number of experimental techniques have shed additional light on the UFD process in such systems.<sup>11–13</sup> Together, these studies provide a solid understanding of the UFD process in the isolated bromomethane molecules.

In HBr molecules, the  $3d \rightarrow \sigma^*$  core excitation puts the molecule in a purely repulsive state.<sup>1</sup> The  $3d \rightarrow 4a_1$  excitation in bromomethane involves similar orbitals, and is also highly repulsive. The Br  $3d$  core-hole lifetime is  $\simeq 6.6$  fs.<sup>14</sup> This time is of the same order of magnitude as the molecular dissociation time in bromomethane (7.1 fs),<sup>2</sup> thus UFD can be observed in the RAS spectra as two overlapping Auger fea-

tures; one from the unfragmented molecules, which we designate  $M_u$ , and one from Auger decays in the atomic Br fragment, designated  $M_f$ . Figure 1 shows a schematic picture of these decay channels (left panel) and also of those in a bromomethane cluster,  $C_{u,f,d}$  (right panel). The notation in the figure will be used throughout the following analysis.

Due to the geometric structure of bromomethane clusters, which will be discussed in further detail together with the calculations, and the high electronegativity of Br, the overall valence electronic structure of the clustered molecules can be affected.

Thus, since the  $3d \rightarrow 4a_1$  excitation is a core-to-valence transition it too can, in principle, be strongly influenced by clustering. We present valence photo-electron spectra (UPS) of the  $2e$  state, X-ray photo-electron spectra (XPS) of the Br  $3d$  level, as well as NEXAFS and RAS spectra where  $3d \rightarrow 4a_1$  excitation has been performed over a range of energies. We performed experiments for both the molecule and for two different cluster sizes. The measurements of the molecular spectra give access to accurate energy calibration and are a necessary reference when analyzing the cluster spectra.

## II. EXPERIMENTAL

The experiments were carried out at the undulator beamline I411 at the MAX-laboratory in Lund, Sweden.<sup>15,16</sup> This beamline is designed to accommodate high-pressure experiments, and is equipped with a hemispherical Scienta R4000 electron energy analyzer for photo-electron spectroscopy. Clusters were produced by adiabatic expansion in a supersonic jet cluster source.<sup>17</sup> A reservoir of liquid bromomethane was connected to the gas inlet system. The vapor of the liquid, with a partial pressure of about 1.9 bars at room temperature, was let directly into the stagnation volume of the cluster source. In the source, the gas was expanded from the stagnation volume through a conical nozzle of 150  $\mu\text{m}$  diameter, with a total opening angle of  $20^\circ$  into the expansion volume. The pressure in the latter volume was kept at around  $10^{-3}$  mbar throughout the experiments. The cluster beam was

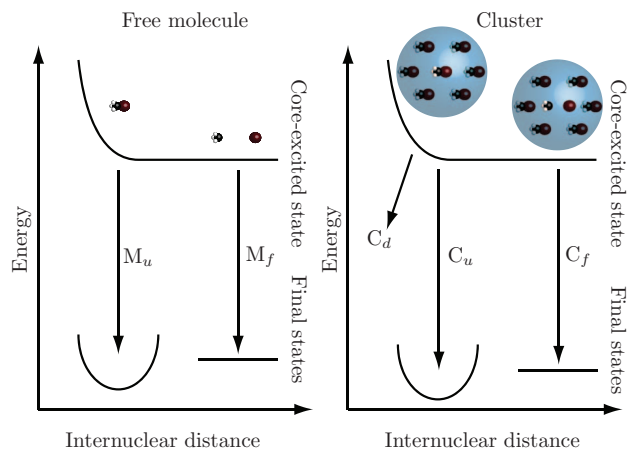


FIG. 1. Schematic picture of the resonant Auger decay pathways in the free molecule (left) and in the cluster (right).  $M_u$  represents Auger decay in the unfragmented free molecule,  $M_f$  represents decay in the free atomic fragment. The pathways designated by  $C$  represents decays taking place in clusters as follows:  $C_u$  is Auger decay in the unfragmented molecule,  $C_f$  is decay in the atomic fragment, and  $C_d$  is a new pathway that can open up due to cluster effects.

skimmed between the expansion volume and the analyzer chamber, enabling a pressure of  $10^{-6}$  mbar to be maintained in the analyzer chamber.

The mean size in the cluster beam was controlled by altering the nozzle temperature by using electrical heating. Three temperatures were used to produce different experimental conditions. At 70 °C, a purely molecular beam was formed. This was used for calibration of the cluster spectra, and to obtain molecular reference spectra. Room temperature ( $\approx 20$  °C) was used to produce large clusters. The size of these clusters corresponds, roughly, to the one used in Ref. 18, i.e., several hundred molecules per cluster. For the smaller size, a temperature of  $\approx 40$  °C was used. XPS spectra were obtained at the different conditions to ensure that the size difference was appreciable between the two cases in a quantitative way. The bromomethane gas was commercially obtained (Fluka,  $\geq 99.5\%$  purity). In the UPS and RAS spectra, the experimental resolution was  $\approx 50$  meV and in the XPS spectra, it was  $\approx 40$  meV. The NEXAFS spectra were acquired using the partial electron yield (PEY) technique, collecting all electrons with a binding energy in the range of 5-45 eV. All spectra were recorded with the electron spectrometer at an angle of  $54.7^\circ$  to the light polarization plane, the so-called magic angle, to avoid angle dependent effects.

### III. CALCULATIONS

To assist with the interpretation of the recorded spectra, we have performed calculations using the *Gaussian 03*<sup>19</sup> quantum chemistry software package. We employed second order Møller-Plesset perturbation theory (MP2) with a cc-PVDZ basis set and the LANL20 effective core potentials during all calculations. A calculation of a realistically sized cluster is not possible at this level of theory. However, bromomethane molecules are known to stack with Pnma symmetry in clusters,<sup>18</sup> putting the Br ends of several molecules close to methyl groups of neighboring ones, and vice versa, and

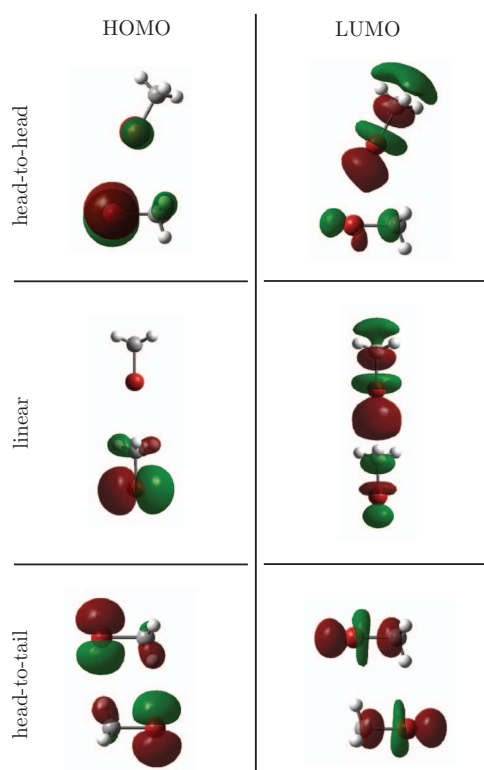


FIG. 2. Iso-surfaces of the HOMO and LUMO in the three dimer geometries. The HOMO probability density is spread over both the constituent molecules except in the linear geometry, and the LUMO is delocalized in all three cases.

linearly in solids at low temperatures. If one can find trends in smaller bromomethane systems with similar geometries, it is reasonable to extrapolate these trends to larger clusters. To this end, we performed geometry optimization and electronic ground state calculations on bromomethane dimers in the three different configurations (head-to-tail, head-to-head, and linear) that the free dimer can attain.<sup>21</sup>

Figure 2 shows iso-surfaces for the highest occupied molecular orbitals (HOMO) as well as the lowest unoccupied molecular orbitals (LUMO) in the three dimer geometries.

It can be seen that for head-to-tail and head-to-head geometry, the  $2e$ -derived HOMO orbitals as well as the LUMO are delocalized over the dimer. For the linear geometry, the unoccupied orbitals are delocalized. Since the Pnma stacking is similar to these geometries, we conclude that the LUMO in bromomethane clusters is probably also delocalized. Further evidence of valence delocalization is offered by the XPS and UPS spectra of bromomethane clusters presented in Sec. IV.

### IV. XPS AND UPS

To be able to quantify if the valence states in bromomethane clusters are delocalized or not, we compare the XPS and UPS spectra from both cluster sizes. The Br 3d XPS line shapes of the clusters were analyzed by applying a Gaussian convolution to the molecular envelope. This was done to take “cluster specific” effects (inter-molecular vibrations, scattering, size distribution, etc.) into account. Figure 3 shows the XPS spectra and fits. For small clusters, the FWHM of the Gaussian was  $\Delta G_s = 0.52$  eV, whereas for the larger

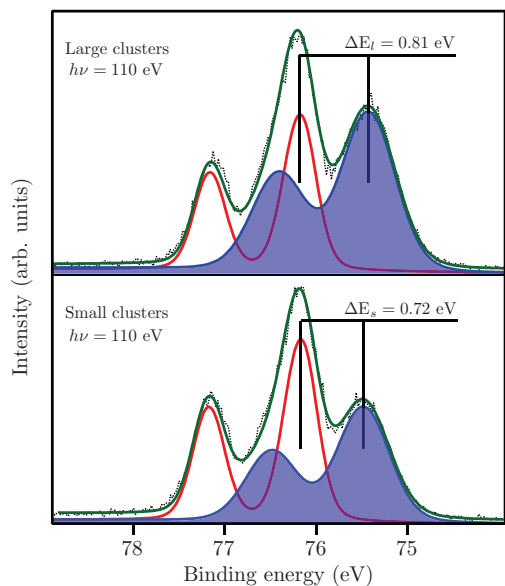


FIG. 3. The Br 3d XPS spectra of large clusters (top), small clusters (bottom). The dotted lines represent experimental data, the red lines are the fitted molecular spectrum, and the shaded areas represent the fitted cluster spectra. The screening shifts  $\Delta E_{l,s}$  are displayed as measured through the fits.

ones it was  $\Delta G_l = 0.57$  eV. The cluster features were also shifted towards a lower binding energy due to polarization screening,<sup>22</sup> this shift was  $\Delta E_s = 0.72$  eV and  $\Delta E_l = 0.81$  eV, respectively. Since XPS probes core levels, which are localized to individual atoms, and UPS probes valence levels, a comparison between the binding energy shifts and line broadenings in these two spectroscopies can yield information about whether the valence states are localized, as in the case of oxygen clusters,<sup>23</sup> or delocalized, as is the case for rare gas<sup>24</sup> and water<sup>25</sup> clusters.

Figure 4 shows the UPS spectrum of large bromomethane clusters. The outermost orbital in bromomethane is the lone-pair  $2e$  orbital, with a very distinct doublet and vibrational structure in the molecule. Provided this orbital is localized to individual molecules, the cluster feature can be fitted using the molecular line-shape, convolved with  $\Delta G_l$ , and shifted by  $\Delta E_l$ . This method was successfully applied in Ref. 23 to describe the outermost valence state in oxygen clusters, and oxygen doped argon clusters.

These fit parameters cannot, however, describe the cluster feature well in the bromomethane case. While the shift remains  $\Delta E_l$ , a significant increase in line-width in comparison to  $\Delta G_l$  is observed;  $\Delta G_{v,l} = 0.91$  eV was measured. The same trend was found to hold for the smaller cluster size, where  $\Delta G_{v,s} = 0.83$  eV was found to produce an accurate fit. These values are roughly 0.3 eV larger than for the XPS lines, and can be explained neither by the difference in experimental resolution ( $\approx 10$  meV), nor by the “cluster specific” broadening.

It has been shown that similar broadening of valence features in rare gas clusters stems from the onset of band formation (i.e., charge delocalization)<sup>24</sup> while in H-bonded water clusters, such a broadening is attributed to a combination of charge delocalization and large geometrical differences be-

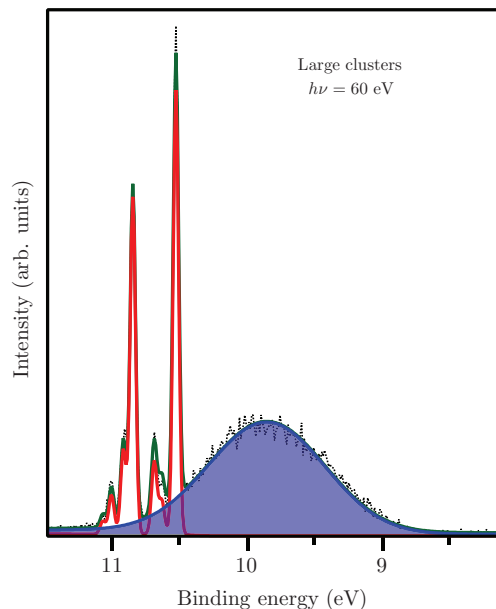


FIG. 4. The UPS spectrum of outermost ( $2e$ ) valence orbital in the bromomethane (red line), and the states in the cluster that are derived from this orbital (shaded blue area).

tween the initial state and ionic final state.<sup>25</sup> In the latter case, the authors observe a large (0.5–0.6 eV) discrepancy between the feature shifts in UPS and XPS spectra, while in the present work, no such difference is observed. This, and the fact that the bonding of the bromomethane clusters is closer in strength and structure to that of van der Waals bonded clusters like oxygen and rare gases, leads us to believe that the main contributing factor in the present case is the formation of a band consisting of the many quasi-degenerate  $2e$ -orbitals of the individual bromomethane molecules.

Further support for this picture is lent by the fact that the largest splitting between the  $2e$  derived molecular orbitals is roughly 0.2 eV. In a simple picture, this splitting can be treated as a lower limit to the valence band width in the clusters, and can account for much of the additional broadening observed in the UPS spectra. Together with the calculated delocalization of the dimer valence states, this is compelling evidence that the outermost valence state in bromomethane clusters is, indeed, delocalized. In Secs. V–VII, we investigate to what extent such initial state effects affect the UFD process.

## V. NEXAFS

The first step in the UFD process is the core-excitation, in this case induced by X-ray absorption. We characterized the absorption spectrum by using NEXAFS. Figure 5 shows the NEXAFS spectra of the bromomethane molecules and large clusters (the molecular contribution to the cluster spectrum is roughly 30%). The kinetic energy window was sufficiently large as to collect all the main resonant Auger features. The spectra have been overlaid, to highlight that within experimental accuracy, there is no difference in the shape of the spectral features. This is in contrast to what is most often observed for clustered molecules, where broadening and shifts are prominent in core-to-valence absorption features.<sup>7,26</sup> The

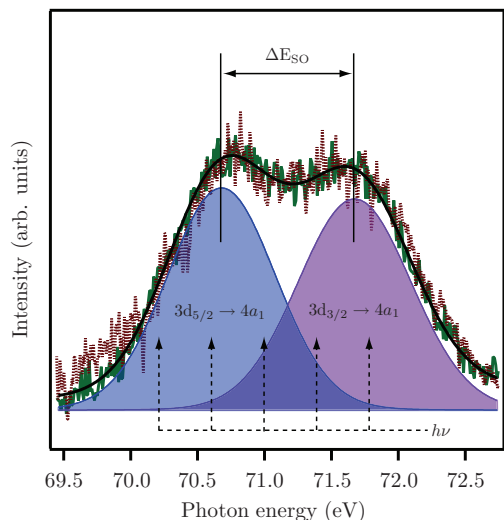


FIG. 5. The Bromomethane  $3d \rightarrow 4a_1$  NEXAFS spectra of the molecule (dotted, brown) and the cluster (solid, green), overlaid. In addition, the two spin-orbit components are shown (shaded areas) as well as the excitation energies used in this work (arrows).

spectral envelope consists of two assignable features, namely, the  $3d_{5/2}$  and  $3d_{3/2}$  spin-orbit components.<sup>2</sup> The spin-orbit splitting was determined to be  $\Delta E_{SO} = 1.0$  eV.

## VI. BROMOMETHANE RAS

In order to investigate the UFD process in bromomethane clusters, we recorded resonant Auger spectra over a range of excitation energies (cf. Fig. 5). Figure 6 shows the molecular RAS spectrum, obtained from the same sample beam as

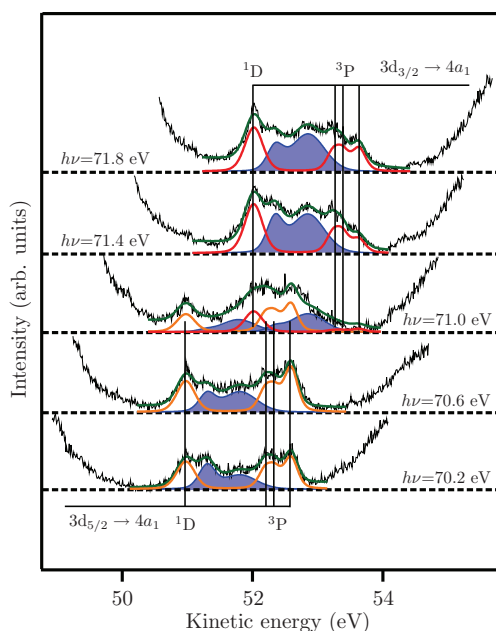


FIG. 6. Molecular RAS spectra at five different excitation energies. The solid lines below each spectrum represent the atomic fragment features ( $M_f$ ;  $3d_{3/2} \rightarrow 4a_1$  in red,  $3d_{5/2} \rightarrow 4a_1$  in orange). The shaded areas represent features that can be assigned to Auger decay in the unfragmented molecules ( $M_u$ ) and to recoil and scattering effects. The green lines show the sum of the fit curves.

the cluster spectra. They match previously reported spectra<sup>2,8</sup> well. The atomic fragment features from UFD (decay channel  $M_f$ ) are clearly visible.

The spectra presented in this work are significantly better resolved than those previously published, and thus additional structure can be observed in the spectral features. We assign these extra features to Auger decay in the unfragmented molecule (decay channel  $M_u$ ; a more detailed analysis using *ab initio* calculations to properly assign the spectrum is beyond the scope of this work) as well as to various recoil and scattering effects that have been shown to affect photoemission line-shapes in general.<sup>27</sup> In the molecular RAS spectra, the feature shift between the two spin-orbit components matches the spin-orbit splitting determined from NEXAFS very well. The relative intensity between the multiplet features ( $^1D$  and  $^3P$  ( $^1S$  is hard to observe, since it overlaps with other spectral features) stemming from the atomic fragments can also be seen to vary between the two spin-orbit components. This variation could be due to interference effects,<sup>28</sup> but is impossible to unambiguously assign without further theoretical treatment.

In order to evaluate the RAS spectra from the clusters, the line-shape analysis was performed with the same methodology as is commonly used when analyzing cluster XPS spectra. This approach was shown to work well in the case of oxygen clusters.<sup>7</sup> Thus, we assume that one can model the cluster line-shapes using the molecular features, shifting them down in binding energy (up in kinetic energy) an amount corresponding to the polarization screening of the final state ion, and applying a Gaussian broadening to take the “cluster specific” effects into account. This is possible, since the polarization screening depends on the charge of the final state ion and the polarizability of the surrounding medium.<sup>22</sup> Because the final states in resonant Auger processes, as in XPS, are singly charged, a good agreement is expected between the RAS shifts and the XPS shifts for the corresponding cluster sizes.

Figure 7 shows RAS spectra of small clusters excited at the same energies as the molecular spectra. It seems that the shift-and-broadening model produces a reasonable fit to the experimental data. We omit the 71.0 eV excitation energy because the many overlapping cluster and molecular features makes the fit less reliable.

For the small cluster size, a binding energy shift of 0.72 eV (see Figure 3) was used, consistent with what was measured in XPS. The cluster line-shapes were convolved with a 0.2 eV Gaussian to take “cluster specific” effects into account. Relative intensities between molecular and cluster components were free parameters in the fits.

Figure 8 shows similar spectra for the larger cluster size. The fitting procedure was conducted in the same way, except for the fact that the binding energy shift used was 0.81 eV, which was the value that was extracted from the corresponding XPS spectrum (see Figure 3). Also in this case, we omit the 71.0 eV excitation energy due to the ambiguities introduced by overlapping spectral features. It should be noted that the fit does not reproduce the spectra for large clusters as well as for small clusters; this might be due to an increase of elastic scattering and/or recoil effects, as well as attenuation of the

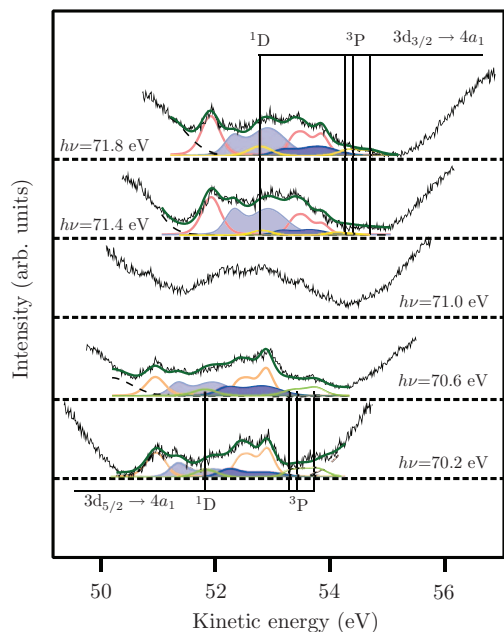


FIG. 7. RAS spectra for small clusters. The excitation energy is given for each spectrum. The two top-most spectra were excited from the  $3d_{3/2}$  spin-orbit component, whereas the bottom two spectra were excited from the  $3d_{5/2}$  component. The middle spectrum was excited where the mixing between the two components was at its maximum. Experimental spectra (black),  $M_f$  (pale red, orange),  $M_u$  (pale blue),  $C_f$  (yellow, light green), as well as  $C_u$  (blue) are plotted as extracted from the line-shape fitting. The green line is the sum of all fit components and the dashed line represents the background, incorporated to reduce fringe effects.

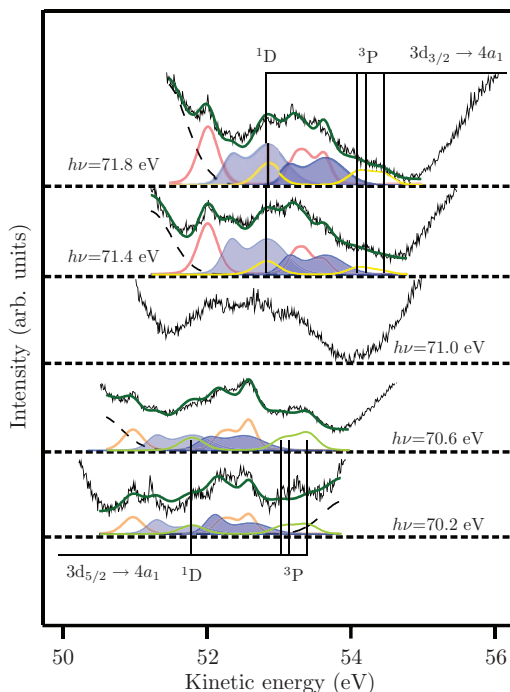


FIG. 8. RAS spectra for large clusters. The excitation energy is given for each spectrum. The two top-most spectra were excited from the  $3d_{3/2}$  spin-orbit component, whereas the bottom two spectra were excited from the  $3d_{5/2}$  component. The middle spectrum was excited where the mixing between the two components was at its maximum. Experimental spectra (black),  $M_f$  (pale red, orange),  $M_u$  (pale blue),  $C_f$  (yellow, light green), as well as  $C_u$  (blue) are plotted as extracted from the line-shape fitting. The green line is the sum of all fit components and the dashed line represents the background, incorporated to reduce fringe effects.

TABLE I. The ratios between decays in the atomic fragment and in the unfragmented molecule for free molecules, small clusters and large clusters. The value for the free molecule matched also what was found for the molecular residue in the cluster spectra. All ratios are given with a precision of  $\pm 0.2$ .

$h\nu$ (eV)	$R_{M_f/M_u}$	$R_{C_f/C_u,small}$	$R_{C_f/C_u,large}$
70.2	2.2	1.2	1.5
70.6	1.6	1.1	1.4
71.4	1.1	0.4	0.6
71.8	1.1	0.5	0.8

outgoing Auger electron by the surrounding cluster. Nonetheless, the deviations are small enough that the previously employed fitting model was deemed sufficient for the analysis.

To be able to quantify differences between the two excitations, between molecules and clusters, and between the separate sizes of clusters, we investigate a number of ratios between the fit components. We define  $N_X$  as the number of decays occurring through channel X (measured through integrated area of the fit components), and the ratio  $R_{X/Y}$ , i.e., the ratio between decays in channels X and Y, as

$$R_{X/Y} = \frac{N_X}{N_Y}. \quad (1)$$

Finally, we define  $R_{sum}$ , that is the total ratio between decays visible in the cluster and the free molecule, as

$$R_{sum} = \frac{N_{C_u} + N_{C_f}}{N_{M_u} + N_{M_f}}. \quad (2)$$

The relevant ratios can be found in Tables I–III. Due to the relatively low signal-to-noise ratio of the RAS spectra, the fragmentation ratios can only be given with a precision of  $\pm 0.2$ , which corresponds to an error bar of roughly to 10%-20%. It can be seen from the values in Table I that within this accuracy, the ratios for each energy point vary only little between the cluster sizes. In both molecular and cluster cases, the ratios are significantly higher for the  $3d_{5/2} \rightarrow a_1$  excitation than for the  $3d_{3/2} \rightarrow a_1$  one. From this, we draw the conclusion that for clusters in this size range, there are no large variations with size in the branching ratios. However, there is a marked difference between the branching ratios of free molecules and molecules in a cluster; i.e.,  $R_{C_f/C_u}$  is consistently smaller than  $R_{M_f/M_u}$ , indicating that the UFD decay channel is suppressed in the clusters.

TABLE II. Ratios between the atomic decays in small clusters and free molecules, between molecular decays in small clusters and free molecules and between the total amount of decays in small clusters and free molecules. All ratios are given with a precision of  $\pm 0.2$ .

$h\nu$ (eV)	$R_{C_f/M_f,small}$	$R_{C_u/M_u,small}$	$R_{sum,small}$
70.2	0.4	0.7	0.5
70.6	0.4	0.7	0.5
71.4	0.2	0.3	0.2
71.8	0.3	0.4	0.3

TABLE III. Ratios between the atomic decays in large clusters and free molecules, between molecular decays in large clusters and free molecules and between the total amount of decays in large clusters and free molecules. All ratios are given with a precision of  $\pm 0.2$ .

$h\nu$ (eV)	$R_{C_f/M_f,large}$	$R_{C_u/M_u,large}$	$R_{sum,large}$
70.2	0.6	1.3	0.8
70.6	0.7	1.2	0.8
71.4	0.2	0.4	0.4
71.8	0.5	0.5	0.6

Tables II and III show another set of ratios, from small and large clusters, respectively, where the individual decay channels for each cluster size are compared as well as the total number of decays within a cluster size as compared to the total number in the free molecules. The first observation from these ratios is that the number of fragment decays in clusters is smaller than the number of fragment decays in the free molecule, while the number of decays in the unfragmented molecule actually increases in the large clusters as compared to the free molecule. This indicates that there is an effect that reduces the dissociative character of the excited state in clusters. Also, it can be readily seen, when comparing the spectra in the Figures 7 and 8, that the cluster features are more prominent for larger clusters. This is expected, since the degree of condensation in the cluster beam is higher in the case of large clusters, thus there will be less molecular residue and more clusters. This is also confirmed by the values  $R_{sum,small}$  and  $R_{sum,large}$ : the ratio of decays in the clusters as compared to free molecules is almost twice as high in the case of large clusters.

For neither cluster size, the ratios in the RAS spectra match those of their XPS counterparts;  $R_{XPS,small} = 1.0$  as compared to  $\bar{R}_{sum,small} = 0.4$  and  $R_{XPS,large} = 1.7$  as compared to  $\bar{R}_{sum,large} = 0.7$ . Thus, the total intensity ratio between Auger decays in clusters and Auger decays in free molecules are less than 50% of the ratio of ionization events seen in molecular and cluster XPS, both for small and large clusters. We do not believe that cross-section changes between the clustered and the free molecules or differences in the mean-free path of the photo- and Auger electrons can account for this large difference. Instead, we attribute this to another, cluster specific decay channel in the cluster RAS,  $C_d$ . This is also supported by the differences in the branching ratios listed in Tables II and III, and by the somewhat surprising fact that the screened fragment decay to free fragment decay ratios ( $R_{C_f/M_f,small}$  and  $R_{C_f/M_f,large}$ ) and the screened unfragmented molecule to the free molecule ratios ( $R_{C_u/M_u,small}$  and  $R_{C_u/M_u,large}$ ) change drastically between the two spin-orbit excitations. This is unexpected, since the NEXAFS spectrum looks similar for the cluster and the molecule, and since the two spin-orbit components have approximately equal absorption intensity in the cluster NEXAFS. A reasonable explanation for this behavior would be that the spectral intensity is redistributed to Auger features inside the PEY energy range, but far away enough from the atomic RAS features as not to be detected in our spectra.

## VII. DISCUSSION

We have measured the UPS, XPS, NEXAFS, and RAS spectra of bromomethane molecules and different size clusters. The polarization screening from a singly charged ion found in the XPS matches what is found also in the RAS and UPS spectra. The ratio between decays in the clusters and free molecules, extracted from the XPS and RAS spectra, show that the amount of fragment decays inside clusters is significantly lower in clusters than in free molecules. At first glance, this is puzzling, since the NEXAFS spectra associated with the  $3d \rightarrow 4a_1$  transitions are virtually identical between clusters and molecules. Such a discrepancy can have several possible explanations. Luckily, it is possible to rule some of these possibilities out *a priori*.

The first such possibility is fragment cage-exit, which would mean that the photo-fragment moves outside of the cluster before the Auger decay takes place. Since the mean flight distance of a Br fragment before a decay occurs is 0.08 Å and the radius of the cluster is several Å, it is straightforward to see that this cannot be a main contributing factor. Recapture of the Auger electron can also be ruled out, since the measured kinetic energy is around 50 eV, and scattering effects would not preferentially suppress one of the spin-orbit components.

Instead, due to the strong support yielded by the experiment and theory for the assumption that both the HOMO and LUMO of  $\text{CH}_3\text{Br}$  clusters are, to an extent, delocalized over the clusters, we propose that the observed decrease in fragment decays inside the clusters, as compared to the free molecules, is mainly due to a delocalization of the intermediate state electron. After photo-excitation, the delocalized nature of the LUMO facilitates charge transfer, away from the molecule where the core hole is located. This lessens the dissociative character of the excited state, and presumably leads to a redistribution of decays to normal Auger channels present only in the clusters ( $C_d$ ), leaving the NEXAFS spectra unchanged. Unfortunately, the redistributed intensity is too small to be readily detected in a wide-range normal Auger spectrum with our experimental setup.

The change in chemical environment and symmetry induced by clustering can also affect the molecular field splitting of the Br  $3d$  component in the initial state. Such effects are known to influence the relative intensities of the molecular field splitting components in other molecules strongly, and can potentially explain the intensity variation between the  $3d_{3/2}$  and  $3d_{5/2}$  components. Together, these two effects account for the, at a first glance, contradictory experimental observations.

Future studies of this and similar systems would benefit greatly from more complex *ab initio* studies of larger molecular clusters, both in the ground and in the core excited state. We encourage further initiatives in this direction. This work highlights the importance of understanding how different bonding mechanisms in molecular clusters leads to different behavior of their excited states, something that might play a key role in, for example, environmental and atmospheric chemistry.

## ACKNOWLEDGMENTS

We acknowledge the financial support of the Knut and Alice Wallenberg foundation, the Swedish Research Council (VR), The Swedish Foundation for Strategic Research (SSF), and the Göran Gustafsson foundation. We also thank the MAX-lab staff for their support during the experiments.

- <sup>1</sup>P. Morin and I. Nenner, *Phys. Rev. Lett.* **56**, 1913 (1986).  
<sup>2</sup>P. Morin and I. Nenner, *Phys. Scr.* **T17**, 171 (1987).  
<sup>3</sup>O. Björneholm, S. Sundin, S. Svensson, R. R. Marinho, A. Naves de Brito, F. Gel'mukhanov, and H. Ågren, *Phys. Rev. Lett.* **79**, 3150 (1997).  
<sup>4</sup>A. Naves de Brito, R. Feifel, A. Mocellin, A. B. Machado, S. Sundin, I. Hjelte, S. L. Sorensen, and O. Björneholm, *Chem. Phys. Lett.* **309**, 377 (1999).  
<sup>5</sup>I. Hjelte, O. Björneholm, V. Carravetta, C. Angeli, R. Cimiraglia, K. Wiesner, S. Svensson, and M. N. Piancastelli, *J. Chem. Phys.* **123**, 064314 (2005).  
<sup>6</sup>P. Morin and C. Miron, *J. Electron Spectrosc. Relat. Phenom.* **185**, 259 (2012).  
<sup>7</sup>T. Rander, M. Lundwall, A. Lindblad, G. Öhrwall, M. Tchapyguine, S. Svensson, and O. Björneholm, *Eur. Phys. J. D* **42**, 253 (2007).  
<sup>8</sup>I. Nenner, P. Morin, P. Lablanquie, M. Simon, N. Levasseur, and P. Millie, *J. Electron Spectrosc. Relat. Phenom.* **52**, 623 (1990).  
<sup>9</sup>T. N. Olney, W. F. Chan, G. Cooper, C. E. Brion, and K. H. Tan, *J. Electron Spectrosc. Relat. Phenom.* **66**, 83 (1993).  
<sup>10</sup>T. N. Olney, G. Cooper, W. F. Chan, G. R. Burton, C. E. Brion, and K. H. Tan, *Chem. Phys.* **218**, 127 (1997).  
<sup>11</sup>R. Bohinc, M. Žitnik, K. Bučar, M. Kavčič, L. Journal, R. Guillemin, T. Marchenko, M. Simon, and W. Cao, *J. Chem. Phys.* **139**, 134302 (2013).  
<sup>12</sup>O. Travnikova, V. Kimberg, R. Flammini, X.-J. Liu, M. Patanen, C. Nicolas, S. Svensson, and C. Miron, *J. Chem. Phys. Lett.* **4**, 2361 (2013).  
<sup>13</sup>M. N. Piancastelli, G. Goldsztejn, T. Marchenko, R. Guillemin, R. K. Kushawaha, L. Journal, S. Carniato, J.-P. Rueff, D. Céolin, and M. Simon, *J. Phys. B* **47**, 124031 (2014).  
<sup>14</sup>T. Matila, R. Püttner, A. Kivimäki, H. Aksela, and S. Aksela, *J. Phys. B* **35**, 4607 (2002).  
<sup>15</sup>M. Bässler *et al.*, *J. Electron Spectrosc. Relat. Phenom.* **101**, 953 (1999).  
<sup>16</sup>M. Bässler *et al.*, *Nucl. Instrum. Methods Phys. Res. A* **469**, 382 (2001).  
<sup>17</sup>M. Tchapyguine, R. Feifel, R. R. T. Marinho, M. Gisselbrecht, S. L. Sorensen, A. Naves de Brito, N. Mårtensson, S. Svensson, and O. Björneholm, *Chem. Phys.* **289**, 3 (2003).  
<sup>18</sup>A. Rosso, T. Rander, H. Bergersen, A. Lindblad, M. Lundwall, S. Svensson, M. Tchapyguine, G. Öhrwall, L. Sæthre, and O. Björneholm, *Chem. Phys. Lett.* **435**, 79 (2007).  
<sup>19</sup>M. J. Frisch, G. W. Trucks, H. B. Schlegel *et al.*, Gaussian 03, Revision C.02, Gaussian, Inc., Wallingford, CT, 2004.  
<sup>20</sup>P. J. Hay and W. R. Wadt, *J. Chem. Phys.* **82**, 299 (1985).  
<sup>21</sup>Y. Futami, S. Kudoh, F. Ito, T. Nakanaga, and M. Nakata, *J. Mol. Struct.* **690**, 9 (2004).  
<sup>22</sup>O. Björneholm, F. Federmann, F. Föcking, and T. Möller, *J. Chem. Phys.* **104**, 1846 (1996).  
<sup>23</sup>T. Rander, A. Lindblad, M. Lundwall, M. Tchapyguine, G. Öhrwall, S. Svensson, and O. Björneholm, *J. Chem. Phys.* **130**, 224305 (2009).  
<sup>24</sup>D. Rolles, H. Zhang, Z. D. Pešić, J. D. Bozek, and N. Berrah, *Chem. Phys. Lett.* **468**, 148 (2009).  
<sup>25</sup>S. Barth, M. Ončák, V. Ulrich, M. Mucke, T. Lischke, P. Slavíček, and U. Hergenbahn, *J. Chem. Phys. A* **113**, 13519 (2009).  
<sup>26</sup>A. A. Pavlychev and E. Rühl, *J. Electron Spectrosc. Relat. Phenom.* **106**, 207 (2000).  
<sup>27</sup>E. Kukk, K. Ueda, and C. Miron, *J. Electron Spectrosc. Relat. Phenom.* **185**, 278 (2012).  
<sup>28</sup>R. Feifel, F. Burmeister, P. Salek, M. N. Piancastelli, M. Bässler, S. L. Sorensen, C. Miron, H. Wang, I. Hjelte, O. Björneholm, A. Naves de Brito, F. K. Gel'mukhanov, H. Ågren, and S. Svensson, *Phys. Rev. Lett.* **85**, 3133 (2000).